Journal of Applied Electrochemistry **33**: 553–561, 2003.

An EXAFS investigation of molybdate-based conversion coatings

J.A. WHARTON[1], D.H. ROSS[2], G.M. TREACY[2], G.D. WILCOX[2] and K.R. BALDWIN[3]
[1]*School of Engineering Sciences, University of Southampton, Highfield, Southampton, Hampshire, SO17 1BJ, Great Britain*
[2]*IPTME, University of Loughborough, Loughborough, Leicestershire, LE11 3TU, Great Britain*
[3]*Mechanical Sciences Sector, DERA Farnborough, Hampshire, GU14 0LX, Great Britain*

Received 20 June 2002; accepted in revised form 2 December 2002

Key words: chromate-replacement, conversion coatings, EXAFS, molybdate, passivation, zinc–nickel alloy

Abstract

The composition of molybdate-based conversion coatings on zinc–nickel alloy electrodeposits was examined by extended X-ray absorption fine structure (EXAFS). The absorption spectra from appropriate standards showed distinct differences between the Mo(IV) and Mo(VI) oxidation states. A pre-edge peak was apparent for the various molybdate species and molybdenum trioxide, with the energy and intensity dependent on the coordination of the molybdenum. A shift in the molybdenum K-edge spectra was also evident between Mo(IV) and Mo(VI) compounds. A qualitative analysis revealed that both Mo(IV) and Mo(VI) species were present within the molybdate-based conversion coating, with a significant prevalence of hexavalent molybdenum.

1. Introduction

Chromate-based passivation treatments have been successfully used as promoters of conversion coatings for many years [1–3]. Their effectiveness is without question although there are many problems with regard to their environmental suitability. Some chromium(VI) compounds are carcinogenic and all are toxic. It is problems such as these that has lead researchers to evaluate other potential systems, of lower toxicity, to ascertain if they can replace chromates as passivators. One such system is that based on molybdate, a group VIA oxy-anion analogue of chromate. Molybdates have been examined by a number of investigators [4–9], although only a few have reported encouraging results. Molybdates are still an attractive class of compounds, however, as they possess strong film-forming abilities on a number of metallic surfaces. It is therefore important to examine the constituency of molybdate passivated surfaces, particularly with respect to the oxidation states of the molybdenum. This information can then be used to aid improvement of their performance. The investigations outlined in this paper are based on molybdate coatings formed on zinc–nickel electrodeposits. This type of zinc alloy coating is now being widely adopted as an effective sacrificial treatment for ferrous surfaces.

In recent years, X-ray absorption near edge spectroscopy (XANES) has been increasingly used as a technique for surface analysis of related coating systems [10–12]. The analysis can be performed under ambient temperatures and pressures, so coatings are unaffected by exposure to an ultra high vacuum and also coatings are less susceptible to photoreduction by the higher energy photons [13, 14], as would be the case for X-ray photoelectron spectroscopy (XPS). XANES measurements involving a glancing incident angle fluorescence technique have been utilized to study the role of chromate [10, 11] and cerium ions [12] as corrosion inhibitors on aluminium and aluminium alloys, resulting in the determination of the valency of species present within the films at low concentrations. Previous investigations on molybdate-based coatings using XPS have indicated the existence of a range of molybdenum oxidation states, including Mo(II) [8], Mo(IV) as MoO_2 [5, 15], Mo(V) [5, 8] and Mo(VI) identified both in the initial surface layers as either MoO_3 or MoO_4^{2-}, [8, 15] and also within the internal layers [13]. The black molybdate coatings produced from ammonium heptamolybdate ($(NH_4)_6Mo_7O_{24} \cdot 4H_2O$) treatments, have similarly been considered to contain a mixture of $MoO(OH)_2$ and MoO_3 [16, 17], with one XPS study suggesting an estimated oxidation state for molybdenum within the black coatings of about +5, which was considered to be close to a Mo_4O_{11} structure [18].

1.1. *X-ray absorption spectroscopy*

The molybdenum K-edge shifts significantly depending on its oxidation state and the local arrangement of the neighbouring atoms around the absorbing atom [19, 20]. Various molybdate species, molybdenum trioxide and several other molybdenum compounds show a pre-edge peak, the energy and intensity of which will depend on the coordination of the molybdenum [21]. For

molybdenum K-edge spectra, the principal transition is the 1s $\rightarrow$ 4d (the excitation of core electrons to vacant orbitals [22]) associated with this pre-edge peak. This transition is much stronger where the molybdenum atom is tetrahedrally coordinated and for those compounds with no centre of symmetry, than where molybdenum is strictly octahedrally coordinated, where this transition is dipole forbidden [23]. The absolute position of the edge features can consequently be utilized to gain information about the chemical environment of the absorber atom [24]. The region up to approximately 40 eV above the absorption edge is referred to as the XANES region. Within this area the simple extended X-ray absorption fine structure (EXAFS) theory breaks down. Nevertheless, XANES can give information about vacant orbitals, the electronic configuration and the site symmetry of the absorbing atom. Moreover, the absolute position of the edge contains information about the oxidation state of the absorber [25, 26], beyond the absorption edge over a range of 50 to 1500 eV in the EXAFS region. The main attraction of this technique is that it provides specific information about the surrounding environment of atoms for a particular element.

2. Experimental methods

Molybdenum K-edge EXAFS data was collected for a range of molybdenum containing compounds and molybdate treated zinc–nickel alloy electrodeposits at the Daresbury Laboratory (SRS) UK. Transmission mode was used for the standards and fluorescence mode for the coated surfaces, on stations 9.2 and 9.3. Ionization chambers were filled with a mixture of Ar/He and Kr/He at the appropriate partial pressures to optimize detector sensitivities. Both detectors were required during the transmission mode, situated in the incident beam path before and behind the standards. The standards were prepared by sandwiching thin, uniform layers of the standard material between thin plastic films, held in position by a rigid frame. For the coated surfaces the fluorescence mode was utilized, in which one ionization chamber was situated before the coated coupon, with a solid state fluorescence detector position at 90° to the beam path. The coupon was positioned at 45° mutually to the incident beam and the fluorescent detector. The Si[220] monochromators on both stations were detuned by 50% to eliminate higher order harmonic photons in the incident beam. All EXAFS data was collected at room temperature and atmospheric pressure. The monochromator molybdenum K adsorption edge position (E_o) for stations 9.2 and 9.3, was calibrated using a molybdenum foil, to establish any difference between the two stations.

Data were analysed using well-established procedures. The programs EXCALIB, EXBACK and EXCURV92 [27] were utilized to extract the EXAFS signal and for the analysis of the data. Least squares refinements of the structural parameters of the standards and coated surfaces were carried out against the k^3 weighted EXAFS signal to minimize the fit index (FI). Interatomic distances for the standard compounds were retrieved from the Chemical Database Service, based at Daresbury Laboratory. Two databases were utilized, the Inorganic Crystal Structure Data file (ICSD) [28] and the Metals Data File (MDF) [28]. Both provide fast retrieval of structural and bibliographic information. To calculate the radial distribution of atoms in a crystal out to a selected distance from a central molybdenum atom, required the Crystal Radial Distribution Calculation program (CRAD) [28]. To obtain the fitted Fourier transform for the standards and coated surfaces, the number of atoms in each shell were fixed, and the shell distances (R) and Debye–Waller factor (A) were refined to give a minimum in the discrepancy index.

2.1. *Standards*

A range of compounds containing molybdenum in different chemical environments and oxidation states were required in order that direct comparisons of molybdenum K-absorption edge spectra and fitted Fourier transform could be made with the coated surfaces. A number of the molybdenum compounds were prepared in the laboratory, as described below, with the remaining standards, Na_2MoO_4, $Na_2MoO_4 \cdot 2H_2O$, $ZnMoO_4$, MoO_3 and MoO_2 being analytical reagent grade.

2.1.1. *Sodium heptamolybdate*

$Na_6Mo_7O_{24}$ was obtained as a white crystalline solid from a $Na_2MoO_4 \cdot 2H_2O$ solution (5 g in 50 cm^3) adjusted to pH 5.0 with H_2SO_4. The solution was allowed to evaporate at room temperature under a reduced pressure [29].

2.1.2. *Dizinc trimolybdenum(IV) oxide*

$Zn_2Mo_3O_8$ was prepared from ZnO and MoO_2, mixed in the required stoichiometric ratios, packed in the form of a pellet and heated in a sealed evacuated silica tube at a temperature of 1045 °C for 144 h [29, 30].

2.1.3. *Trizinc dimolybdenum(VI) oxide*

$Zn_3Mo_2O_9$ was prepared from ZnO and MoO_3, mixed in the required stoichiometric ratios, packed in the form of a pellet and heated in a sealed evacuated silica tube at a temperature of 905 °C for 144 h [31].

2.2. *Coated surfaces*

The molybdate coated surfaces were prepared on zinc–nickel alloy electrodeposits, using 50 mm $\times$ 50 mm sized mild steel coupons and a proprietary plating solution. The zinc–nickel alloy plating solution composition included 30 g l^{-1} of both zinc and nickel (as metal), the process operated at a temperature between 38–40 °C, pH 5.6–6.0, a current density of 10 A dm^{-2} and

was agitated by continuous aeration, producing a nominal electrodeposit thickness of 8 μm. The composition of the electrodeposits was within a range of 10 to 14 wt % nickel. Actual electrodeposits were within a range of 10 to 14 wt % nickel, with a nominal thickness of 8 μm. The molybdate coatings were obtained by immersion of the coupons into a 0.1 M (24.1 g l^{-1}) $Na_2MoO_4 \cdot 2H_2O$ at 40 °C and pH 3.0 [9]. Treatment times were 300 s. These coatings had a thick matt black surface finish.

3. Results and discussion

Figure 1 shows the normalized EXAFS spectra for the standard molybdenum containing compounds. Also the positions of the pre-edge peaks, edge and relative edge positions with respect to molybdenum foil, determined within the EXBACK routine during background subtraction, can be seen in Table 1. From a qualitative analysis of the spectra, a considerable amount of information can be obtained concerning the chemical environment of the molybdenum. The molybdenum K-edge shifts significantly depending on its oxidation state and the local arrangement of the neighbouring atoms around the absorbing atom [19, 20]. The molybdenum K-absorption edge for sodium molybdate dihydrate ($Na_2MoO_4 \cdot 2H_2O$) (spectrum (a)), revealed a characteristic pre-edge peak at an energy of 20 002.8 eV, corresponding to the excitation of a core electron to a high level vacant orbital, a $1s \rightarrow 4d$ transition [22, 23]. In a tetrahedral field (sp^3 hybridization) this transition is permitted, although a similar pre-edge peak is also observed in compounds with molybdenum in a distorted octahedral field. However, in a strictly octahedral field (d^2sp^3 hybridization) this transition is forbidden. The anhydrous sodium molybdate (spectrum (b)) as expected revealed a high intensity pre-edge peak at 20 002.8 eV, with the edge position at 20 014.8 eV. A second pre-edge peak was also clearly distinguishable at a higher energy, possibly as a consequence of a $1s \rightarrow 5p$ transition [32]. Overall, the spectrum for anhydrous sodium molybdate had greater detail due to the absence of neighbouring H_2O which attenuates the absorption spectrum. The molybdenum K-absorption edge for the molybdenum trioxide (MoO_3) showed a low intensity pre-edge peak at 20 004.9 eV (spectrum (c)), at a slightly higher energy than the pre-edge peak for Na_2MoO_4. Structurally, MoO_3 represents a transitional stage between tetrahedral and octahedral coordination, resulting in a distorted octahedral symmetry [33]. The pre-edge peak is shifted to a higher energy due to the distortion of the octahedral arrangement. However, the overall edge position at 20 013.6 eV, is slightly lower in comparison with Na_2MoO_4. The molybdenum K-absorption edge for sodium heptamolybdate (spectrum (d)), indicated the presence of a low intensity pre-edge peak at 20 004.5 eV and the edge position at 20 013.4 eV. The energy of the pre-edge peak and edge appear to be similar when compared with the MoO_3 spectra, which suggests that the heptamolybdate species has a coordination similar to a distorted octahedral symmetry [34]. The molybdenum dioxide (spectrum (e)) has a K-absorption edge of 20 011.5 eV; the absence of any

Table 1. Comparisons in the pre-edge position and edge position (E_o) for molybdenum containing standards
$E_{o,Mo}$: Edge position for molybdenum foil.
*EXAFS spectra measured on station 9.2, with the remainder on station 9.3.

Sample	Pre-edge position /eV	Edge position E_o /eV
Sodium molybdate dihydrate	20 002.8	20 014.9
Sodium molybdate anhydrous	20 002.8	20 014.8
Molybdenum trioxide	20 004.9	20 013.6
Sodium heptamolybdate	20 004.5	20 013.4
Molybdenum dioxide	–	20 011.5
Zinc molybdate	20 003.2	20 015.0
Dizinc trimolybdenum(IV) oxide*	–	20 010.1
Trizinc dimolybdenum(VI) oxide*	20 003.6	20 015.1
Molybdate-based coating	20 004.5	20 011.1
Molybdenum foil (station 9.2), $E_{o,Mo}$	–	20 008.4
Molybdenum foil (station 9.3), $E_{o,Mo}$	–	20 008.1

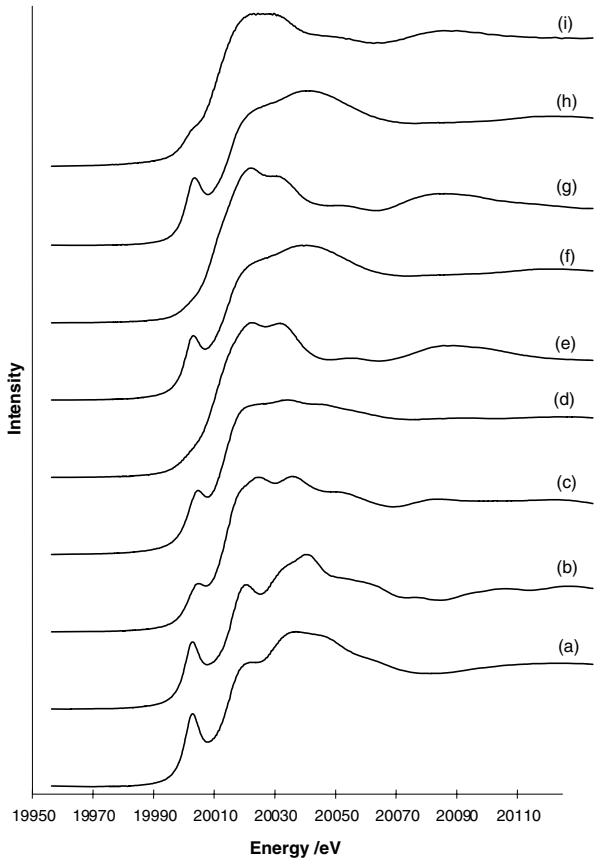

Fig. 1. Normalized experimental EXAFS spectra for: (a) sodium molybdate dihydrate, (b) sodium molybdate anhydrous, (c) molybdenum trioxide, (d) sodium heptamolybdate, (e) molybdenum dioxide (f) zinc molybdate, (g) dizinc trimolybdenum(IV) oxide, (h) trizinc dimolybdenum(VI) oxide and (i) the molybdate-based coating.

Table 2. Occupation numbers (N), distances (R) derived from the single-crystal structure for the standards and molybdate-based coating, and the EXAFS-derived distances and Debye–Waller factors (A)

Compound	Shell	N	Crystallographic-derived, R/Å	EXAFS-derived R/Å	A/Å^2
$NaMoO_4 \cdot 2H_2O$	Mo–O	4	1.770	1.771	0.002
$NaMoO_4$	Mo–O	4	1.770	1.792	0.003
	Mo··Na	7	3.716	3.742	0.007
	Mo··O	8	3.993	4.079	0.013
	Mo··Mo	4	4.359	4.409	0.024
MoO_3	Mo–O	2	1.702	1.578	0.021
	Mo–O	4	2.119	2.190	0.003
	Mo··Mo	2	3.437	3.273	0.017
	Mo··Mo	4	3.829	3.871	0.004
	Mo··Mo	8	4.088	4.113	0.021
$Na_6Mo_7O_{24}$	Mo–O	2	1.730	1.706	0.006
	Mo–O	2	1.960	1.946	0.008
	Mo–O	2	2.232	2.254	0.019
	Mo··Mo	3	3.300	3.298	0.012
	Mo··Na	2	3.811	3.644	0.019
MoO_2	Mo–O	4	1.983	1.980	0.019
	Mo–O	2	2.059	2.000	0.003
	Mo··Mo	1	2.510	2.513	0.004
	Mo··Mo	1	3.112	3.123	0.006
	Mo··Mo	8	3.708	3.693	0.010
	Mo··Mo	20	5.483	5.503	0.015
$ZnMoO_4$	Mo–O	4	1.772	1.752	0.010
	Mo··Zn	3	3.414	3.404	0.021
	Mo··Zn	3	3.613	3.531	0.018
$Zn_2Mo_3O_4$	Mo–O	2	1.906	1.903	0.007
	Mo–O	4	2.081	2.045	0.005
	Mo–Mo	2	2.529	2.526	0.003
	Mo··Mo	2	3.246	3.245	0.008
	Mo··Zn	3	3.748	3.486	0.017
$Zn_3Mo_2O_9$	Mo–O	4	1.756	1.756	0.013
Molybdate-based	Mo–O	2.0	1.730	1.623	0.008
coating	Mo–O	2.0	1.928	1.839	0.023
	Mo–O	3.2	2.118	2.006	0.008
($Zn_2Mo_3O_4$ and $Na_6Mo_7O_{24}$)	Mo··Mo	1.2	2.529	2.546	0.006
	Mo··Zn	0.6	3.107	3.047	0.008

pre-edge peak indicates that a strictly octahedral field exists (d^2sp^3 hybridization). The $1s \rightarrow 4d$ transition is forbidden in octahedral symmetry and consequently no pre-edge peak was evident in this spectrum. The molybdenum K-absorption edge for zinc molybdate ($ZnMoO_4$) revealed a characteristic pre-edge peak of moderate intensity at 20 003.2 eV (spectrum (f)), with the adsorption edge position at an energy of 20 015.0 eV, consistent with its tetrahedral symmetry, whereas, for the dizinc trimolybdenum(IV) oxide, $Zn_2Mo_3O_8$, (spectrum (g)), only an edge position of 20 010.1 eV was apparent. With no pre-edge peak evident, this suggests a strictly octahedral field. Comparing the absorption spectra of $Zn_2Mo_3O_8$ and MoO_2 shows that although both are octahedral in arrangement, differences in the chemical environment are apparent for the $Zn_2Mo_3O_8$, as indicated by the post edge structure. Similarly, the trizinc dimolybdenum(VI) oxide, $Zn_3Mo_2O_9$, (spectrum (h)), revealed a moderately intense pre-edge peak at an energy of 20 003.6 eV. When compared with MoO_3, the lower energy of the pre-edge peak suggests a change of symmetry had occurred, from the distorted octahedral of MoO_3 to a tetrahedral field, similar in arrangement to the molybdate species.

The standard EXAFS shell and radial distribution data of atoms surrounding the central molybdenum atom were determined as explained in the experimental section. The results are shown in Table 2. The details of the number of shells and other structural parameters used for each standard can be seen; Mo–X represents a physical bond and Mo··X indicates a neighbouring shell with a backscattering interaction (where X=O, Mo, Na or Zn). Omitted shells had no statistical significance or visual effect on the calculated Fourier transform. The experimental Fourier transform and the theoretical fit for sodium molybdate dihydrate can be seen in Figure 2. Interatomic distances from the single crystal X-ray

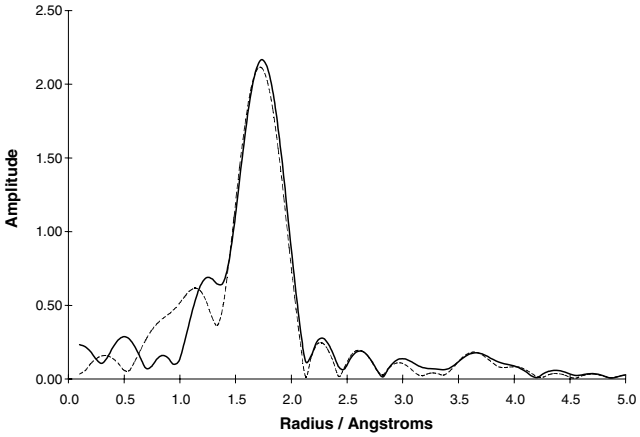

Fig. 2. Experimental (——) and theoretical (- - - -) Fourier transforms for $Na_2MoO_4 \cdot 2H_2O$.

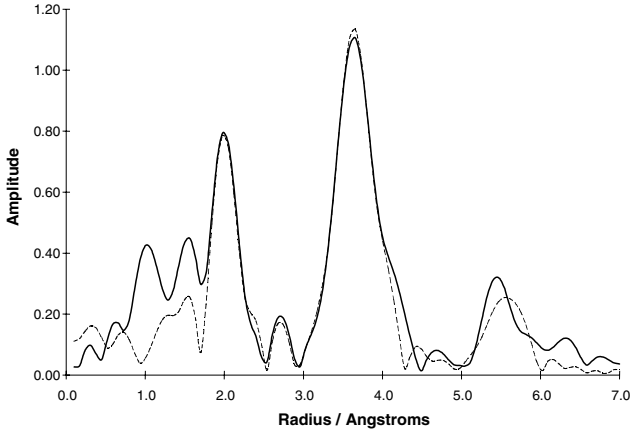

Fig. 4. Experimental (——) and theoretical (- - - -) Fourier transforms for MoO_3.

structure of Matsumoto et al. [35] were used to construct the model. Only the initial oxygen shell could be resolved due to the absence of any further distinctive maxima which could be aligned with theoretical shells. The analysis of the EXAFS data was consistent with a tetrahedral arrangement of four oxygen atoms in the first shell at a distance of 1.771 Å. The experimental Fourier transform for sodium molybdate anhydrous (Figure 3), provided further information to distances of approximately 4.0 Å. The theoretical fit calculated with the additional shells of sodium and oxygen at the correct crystallographic determined distances [35] (Mo··Na 3.716 Å, Mo··O 3.993 Å) is very similar to the experimental data, consistent with the crystalline Na_2MoO_4 containing discrete nearly ideal MoO_4 tetrahedra [31].

The calculated transform for molybdenum trioxide (Figure 4) required the presence of two oxygen shells each containing two and four oxygen atoms respectively (averaged crystallographic distances of 1.702 and 2.119 Å). With the oxygen atoms at slightly different distances from the molybdenum, the experimental MoO_3 data is consistent with the crystallographic studies [36] which have concluded a distorted octahedral symmetry. Additional shells of Mo··Mo interactions (3.437, 3.829 and 4.088 Å) were refined to a distance of 5.5 Å which achieved good agreement with the single crystal X-ray structure [36]. The experimental and theoretical Fourier transforms for sodium heptamolybdate can be seen in Figure 5. The crystallographic determined shell distances suggest a distorted octahedral arrangement, with the first three shells each containing two oxygen atoms at 1.730, 1.960 and 2.232 Å. Overall, there appears to be good agreement between the distances obtained from the EXAFS data and single crystal studies, consistent with the sodium heptamolybdate structure possessing molybdenum in a distorted octahedral arrangement [34].

The experimental and theoretical Fourier transforms for molybdenum dioxide, in Figure 6, indicate good agreement between the shell distances obtained from the crystallographic determined distances and the theoretical fit, with two shells refined for six oxygen atoms (Mo–O, 1.983 and 2.059 Å) [37]. The first EXAFS-derived shell containing four oxygen atoms at 1.980 Å, with the second containing two oxygens at 2.000 Å. This arrangement is consistent with the strictly octahedral

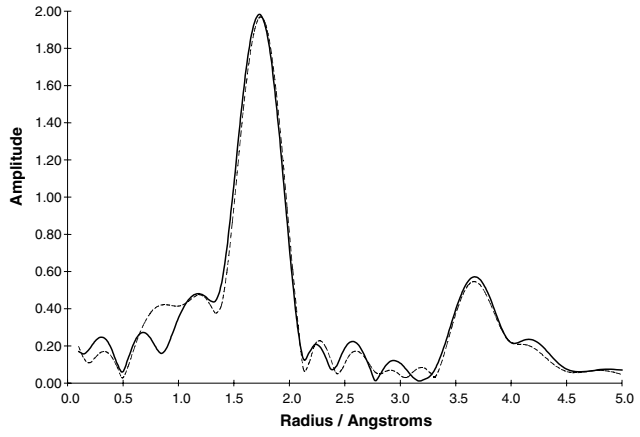

Fig. 3. Experimental (——) and theoretical (- - - -) Fourier transforms for Na_2MoO_4.

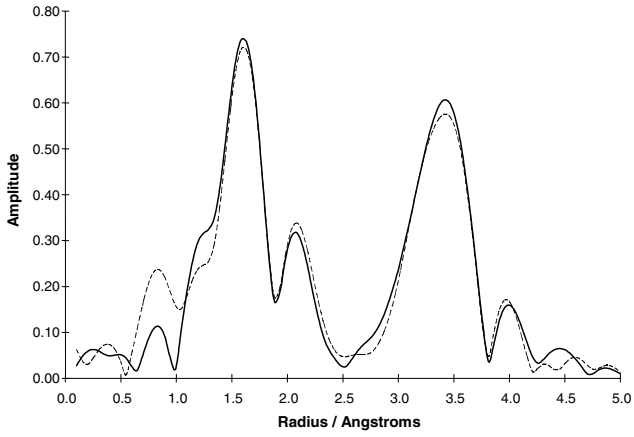

Fig. 5. Experimental (——) and theoretical (- - - -) Fourier transforms for $Na_6Mo_7O_{24}$.

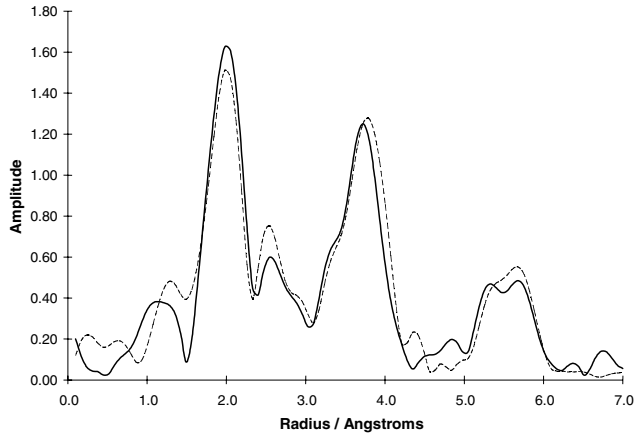

Fig. 6. Experimental (——) and theoretical (- - - -) Fourier transforms for MoO_2.

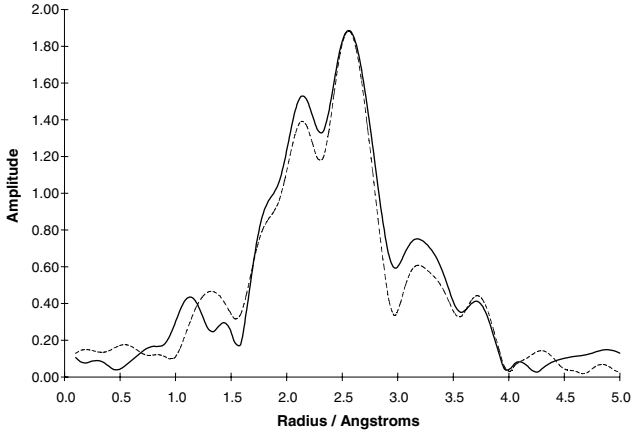

Fig. 8. Experimental (——) and theoretical (- - - -) Fourier transforms for $Zn_2Mo_3O_8$.

symmetry for MoO_2. Additional Mo··Mo shells were refined to a distance of 5.5 Å. The single crystal X-ray studies by Abrahams [38] indicate that zinc molybdate has a tetrahedral arrangement of four oxygen atoms in the first shell at a distance of 1.772 Å, similar to sodium molybdate dihydrate (Figure 7). Additional zinc containing shells could be refined to a distance of 3.6 Å. The experimental transform appeared to be in agreement with the crystallographic studies. For dizinc trimolybdenum(IV) oxide the interatomic distances from the single crystal X-ray structure [30, 39] and also EXAFS data [29] were utilized to refine the theoretical transform.

Figure 8 shows the experimental and theoretical Fourier transforms. The initial oxygen shells at 1.906 and 2.081 Å, in addition to shells of molybdenum and sodium at the correct crystallographic determined distances (Mo–Mo, 2.529 Å and Mo··Mo 3.246 Å, Mo··Na 3.748 Å). The first two oxygen shells containing six oxygen atoms represent a distorted octahedral arrangement, maintaining the configuration from the molybdenum dioxide. There is also evidence of two molybdenum neighbours at 2.526 Å, resulting from a triangular Mo_3O_{13} cluster arrangement, which is know to occur in mixed-metal oxides containing molybdenum [29]. Additional molybdenum and zinc containing shells were refined out to a distance of approximately 4.0 Å. Although the calculated and experimental transforms for $Zn_2Mo_3O_8$ are not as well-defined, the alignments of the peaks are good and compare well with the data obtained by Hibble and Fawcett [29]. The radial distribution data for trizinc dimolybdenum(VI) oxide obtained from the crystallographic studies [31], remains as yet unavailable. However, the authors reported that $Zn_3Mo_2O_9$, has molybdenum surrounded tetrahedrally by four oxygen atoms at an average distance of 1.756 Å.

With only limited amount of data to establish a theoretical fit, the Fourier transform shown in Figure 9, indicates the tetrahedral arrangement in the first shell of Mo–O at a distance of 1.756 Å. Additional shells were also apparent, however, at present the radial distribution remains uncalculated. A comparison with the calculated and experimental transform for MoO_3 (Figure 6), clearly establishes that the $Zn_3Mo_2O_9$ has undergone a radical change in chemical environment; the MoO_3, possesses a distorted octahedral symmetry, whereas the $Zn_3Mo_2O_9$ is tetrahedral in arrangement.

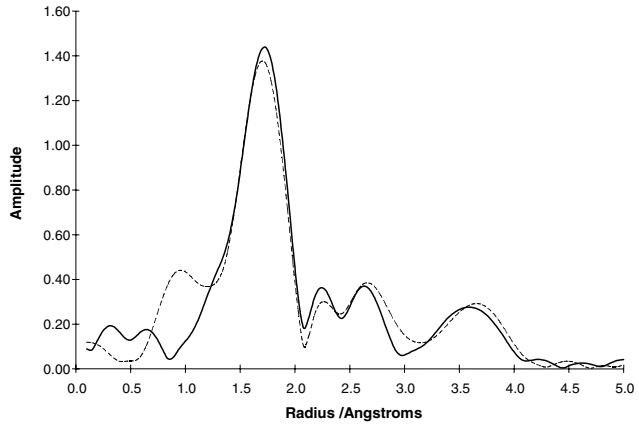

Fig. 7. Experimental (——) and theoretical (- - - -) Fourier transforms for $ZnMoO_4$.

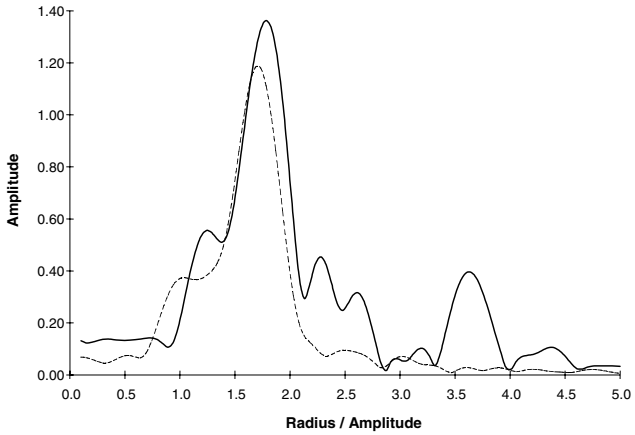

Fig. 9. Experimental (——) and theoretical (- - - -) Fourier transforms for $Zn_3Mo_2O_9$.

3.1. *Molybdate coating*

The molybdenum K-absorption edge for the molybdate-based coating, Figure 1, resulted in a relative edge position of 3.0 eV, similar to the positions measured for MoO_2 (3.4 eV) and $Zn_2Mo_3O_8$ (1.7 eV) as shown in Table 1. If the edge position (E_o) is solely considered, then the adsorption edge would appear to correspond to a strictly octahedral arrangement, suggesting the coating contained tetravalent molybdenum. However, an inflection point (shoulder) on the edge is apparent at an energy of 20 004.5 eV. The energy of this feature is consistent with a pre-edge peak and is not an edge position which are situated at higher energies between 20 010–20 015 eV. The observed pre-edge implies the presence of hexavalent molybdenum within the molybdate-based coating. The measured pre-edge positions for the standards (Table 1) range between 20 002.8 and 20 004.9 eV, with the lower values relating to regular tetrahedral systems such as sodium molybdate, whereas an increasing energy indicates a distorted octahedral symmetry. The absorption spectra can therefore be considered to be the combination of two molybdenum environments, one tetravalent, for example $Zn_2Mo_3O_8$, and the other a distorted hexavalent environment, such as a heptamolybdate species.

The experimental and theoretical Fourier transforms (Figure 10) and the EXAFS data (spectrum (i) in Figure 1 and Table 2) for a molybdate-based coating revealed two relatively broad peaks at distances of approximately 2.0 and 2.6 Å. In fitting the experimental transform, the first peak was considered to be a combination of the Mo–O shells from the two molybdenum environments, with the second peak corresponding to a Mo–Mo interaction at 2.529 Å. The Mo–Mo interaction was most apparent for the $Zn_2Mo_3O_8$; a Mo··Mo interaction was also apparent for MoO_2, however it was significantly weaker. Refinements were consequently undertaken employing different ratios of $Zn_2Mo_3O_8$ and sodium heptamolybdate, utilizing averaged shell distributions and occupancies out to a distance of 3.0 Å, a value dictated by the reliability of the data (lack of signal) at greater distances. By combining shells with similar distances from the two molybdenum environments and varying the occupancy within the resultant shells, different ratios corresponding to different compositions were calculated. An overall best fit was achieved with the experimental data using a ratio of 60% Mo(IV) as $Zn_2Mo_3O_8$: 40% Mo(VI) as the heptamolybdate species, suggesting the presence of a significant quantity of hexavalent molybdenum in the conversion coating. However, this can only be assumed to be an approximate estimation of the relative composition of the hexavalent molybdenum species within the coating.

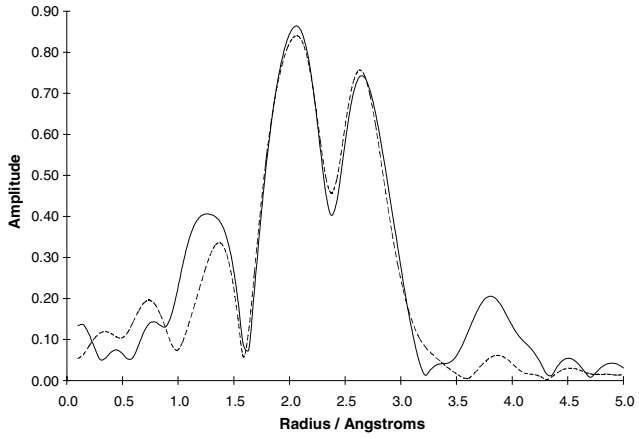

Fig. 10. Experimental (——) and theoretical (- - - -) Fourier transforms for the molybdate-based coating.

An alternative approach to evaluate the coating composition relies on the assumption of a linear relationship between the K-absorption edge positions (E_o) [40]. A linear extrapolation could consequently provide an estimate of the approximate composition of the coated surfaces. Using the relative edge positions, E_R, the Mo(VI) content within the coatings can be calculated, where $Zn_2Mo_3O_8$ has a relative edge position of 1.7 eV; the heptamolybdate species has a position of 5.3 eV (Table 1).

The thus estimated hexavalent molybdenum content in the molybdate-based coating is therefore 36% relative to the total molybdenum. The two methods of estimation gave similar results, suggesting with a degree of confidence that the molybdate-based coating contains significant proportion of hexavalent molybdenum between 30 to 40% relative to the total molybdenum content.

For chromate conversion coatings the generally agreed coating mechanism involves an initial dissolution of the substrate surface, with a corresponding evolution of hydrogen, followed by a reduction of the chromate species to Cr(III) at the metal–solution interface [5, 41, 42]. Proprietary chromate conversion coating treatments contain accelerators such as ferricyanide for redox mediation, which greatly increases the reduction of Cr(VI) to Cr(III) [43]. The dissolution of the substrate increases the local pH at the cathodic sites, resulting in the precipitation of a hydrated mixed oxide, entrapping a residual amount of hexavalent chromium. Although, the hexavalent chromium content within a coating is substrate dependent, for instance, there is no evidence of Cr(VI) on tinplate from industrial chromate processes and for zinc a Cr(VI) composition of between 7–12% has been observed [44]. Previous XANES investigations have established that chromate conversion coatings on aluminium alloys (2024-T3 and 3003-H14) and pure aluminium had a hexavalent chromium to total chromium of approximately 10–20 and 30%, respectively [10, 11], suggesting that hexavalent chromium was a major constituent of the chromate conversion coatings. These two XANES studies used a calibration curve method, defining the pre-edge peak height relative to the edge intensity plotted as a function of the percentage of hexavalent chromium.

Considering an analogous coating mechanism for the molybdate-based coating treatments, in the acidified molybdate solutions, two reactions could occur in parallel at the zinc–nickel alloy surface, involving an initial dissolution of zinc to Zn^{2+}, with an accompanying evolution of hydrogen. Secondly, at the metal–solution interface the reduction of the molybdate species, from Mo(VI) to Mo(IV) could then take place. The local pH will increase at cathodic sites due to the evolution of hydrogen, consequently precipitation of a hydrated mixed zinc and molybdenum oxide could then proceed, entrapping a residual amount of the hexavalent molybdenum. If the formation of the mixed oxide resulted in a structure similar to $Zn_2Mo_3O_8$, then an overall reaction, such as considered in Equation 1, could occur for the molybdate-based coating treatment to form the mixed zinc and molybdenum oxide:

$$14\,Zn^{2+} + 3\,[Mo_7O_{24}]^{6-} + 32\,H^+ + 42\,e^- = 7\,Zn_2Mo_3O_8 + 16\,H_2O \quad (1)$$

The precipitation mechanism is consistent with the observed pH dependency for the coating formation. Increasing the acidity of the treatment solutions increases the rate of coating formation. This corresponds well with the visual observations, where it was evident that the pH 3.0 molybdate treatments resulted in a matt black surface finish, compared with an iridescent colouration when the treatment pH is higher [9]. The entrapped hexavalent molybdenum species within the coating has only a weak oxidising capability compared to hexavalent chromium. The molybdate-based coating could therefore only provide a physical barrier to corrosion, with probably little or no self-healing ability capable of providing enhanced barrier properties to damaged or weak areas within the coating.

4. Conclusions

Absorption spectra from appropriate standards showed distinct differences between the Mo(IV) and Mo(VI) oxidation states. A pre-edge peak was apparent for the various molybdate species and molybdenum trioxide, with the energy and intensity dependent on the coordination of the molybdenum. By utilizing both the molybdenum K-edge positions and EXAFS, the results revealed that the molybdate-based coatings on the zinc–nickel alloy electrodeposit consist of a mixed zinc and molybdenum(IV) oxide, with a significant quantity of hexavalent molybdenum entrapped within the coating. It has been established that the molybdenum(VI) species with the coating had a distorted octahedral arrangement, consistent with the presence of a heptamolybdate species rather than molybdate, MoO_4^{2-}, which has a tetrahedral symmetry. Qualitative analysis revealed the approximate coating composition using two methods, a shell occupancy and a linear extrapolation method, both of which indicated a ratio of hexavalent to total molybdenum content of between 30 to 40%.

Acknowledgements

This work was supported by the Defence Evaluation and Research Agency (DERA) Farnborough. The authors gratefully acknowledge the use of stations 9.2 and 9.3 at the Engineering and Physical Science Research Council (EPSRC) Synchrotron Radiation Source (SRS), Daresbury Laboratory, UK and also the use of the EPSRC Chemical Database Service, also at Daresbury.

References

1. L. Fedrizzi, L. Ciaghi, P.L. Bonora, R. Fratesi and G. Roventi, *J. Appl. Electrochem.* **22** (1992) 247.
2. R. Fratesi, G. Roventi, C. Branca and S. Simoncini, *Surf. Coat. Technol.* **63** (1994) 97.
3. L.F.G. Williams, *Surf. Technol.* **5** (1977) 105.
4. D. Bijimi and D.R. Gabe, *Br. Corros. J.* **28** (1983) 88.
5. G.D. Wilcox, D.R. Gabe and M.E. Warwick, *Corros. Sci.* **28** (1988) 577.
6. D.R. Gabe and S.E. Gould, *Surf. Coat. Technol.* **35** (1988) 79.
7. D.R. Cowieson and A.R. Scholefield, *Trans. Inst. Metal Finish.* **63** (1985) 56.
8. P.T. Tang, G. Bech-Nielsen and P. Møller, *Plat. Surf. Finish.* **81** (11) (1994) 20.
9. J.A. Wharton, G.D. Wilcox and K.R. Baldwin, *Trans. Inst. Metal Finish.* **74** (1996) 210.
10. M.W. Kendig, A.J. Davenport and H.S. Isaacs, *Corros. Sci.* **34** (1993) 41.
11. J. Wan, G.E. Thompson, K. Lu and C.J.E. Smith, *Physica B* **208–209** (1995) 511.
12. A.J. Davenport, H.S. Isaacs and M.W. Kendig, *Corros. Sci.* **32** (1991) 653.
13. A.G. Schrott, G.S. Frankel, A.J. Davenport, H.S. Isaacs, C.V. Jahnes and M. Russak, *Surf. Sci.* **250** (1991) 139.
14. G.P. Halada and C.R. Clayton, *J. Electrochem. Soc.* **138** (1991) 2921.
15. K.P. Han and J.L. Fang, *Surf. Coat. Technol.* **88** (1996) 178.
16. R. Hosseini, B.E. Smith and J.K. Critchley, *Surf. Technol.* **20** (1983) 321.
17. O.P. Agnihotri, K.K. Smith, A.K. Agarwal and V.P. Bhatnagar, *Thin Solid Films* **109** (1983) 193.
18. F. Jahan and B.E. Smith, *Mater. Sci.* **27** (1992) 625.
19. B. Lengeler, *Adv. Mater.* **2** (1990) 123.
20. B. Lengeler, *Phys. B1.* **86** (1990) 56.
21. B.S. Clausen, B. Lengeler and H. Topsøe, *Polyhedron* **5** (1986) 199.
22. R.G. Salman, *Proc. Acad. Sci. USA* **73** (1976) 1384.
23. J. Evans and J.F. Mosselmans, *J. Am. Chem. Soc.* **112** (1991) 3737.
24. S.P. Cramer, T.K. Eccles, F.W. Kutzler, K.O. Hodgons and L.E. Mortenson, *J. Am. Chem. Soc.* **98** (1976) 1287.
25. J.C.J. Bart and G. Vlaic, *Advances in Catalysis* **35** (1987) 3.
26. E.A.V. Ebsworth, D.W.H. Ranfin and S. Cradock, 'Structural Methods in Inorganic Chemistry' 2nd edn, (Blackwell, UK, 1994).
27. N. Binsted, J.W. Campbell, S.J. Gurman and P.C. Stephenson, *EXCURV92, EXAFS Analysis Program*, Central Laboratory of the Research Councils (CLRC) Daresbury Laboratory, Warrington Cheshire, WA4 4AD, UK (1992).

28. The United Kingdom Chemical Database Service, D.A. Fletcher, R.F. McMeaking and D. Parkin, *J. Chem. Int. Comput. Sci.* **36** (1996) 746.
29. S.J. Hibble and I.D. Fawcett, *Inorg. Chem.* **34** (1995) 500.
30. G.B. Ansell and L. Katz, *Acta Crystallogr.* **21** (1967) 482.
31. T. Söhnel, W. Reichett, H. Opperman, Hj. Mattaucsh and A. Simon, *Z. Anorg. Allg. Chem.* **622** (1996) 1274.
32. N-S. Chiu, S.H. Bauer and M.F.L. Johnson, *J. Catalysis* **89** (1984) 226.
33. N.F.D. Verbruggen, G. Mestl, L.M.J. Von Hippel, B. Lengeler and H. Knözinger, *Langmuir* **10** (1994) 3063.
34. K. Sjöbom and B. Hedmen, *Acta Chem. Scand.* **27** (1973) 3673.
35. K. Matsumoto, A. Kobayashi and Y. Sasaki, *Bull. Chem. Soc. Japan* **48** (1975) 1009.
36. L. Kihborg, *Ark. Kemi* **21** (1963) 357.
37. B.P. Branett and A.C. Skapski, *Acta Chem. Scand.* **21** (1967) 661.
38. S.C. Abrahams, *J. Chem. Phys.* **20** (1983) 88.
39. G.B. Ansell and L. Katz, *Acta Crystall.* **1** (1967) 1948.
40. J.F. Mosselmans (Daresbury Laboratory), private communication.
41. L.F.G. Williams, *Surf. Tech.* **4** (1976) 355.
42. K.G. McLaren, J.H. Green and A.H. Kingsbury, *Corros. Sci.* **1** (1961) 61.
43. L. Xia and R.L. McCreery, *J. Electrochem. Soc.* **146** (1999) 3696.
44. W. Huber, *Techn. Rundschau* (*Bern*) **48** (1956) 17. Cited in T. Biestek and J. Weber, 'Electrolytic and Chemical Conversion Coatings a Concise Survey of Their Production, Properties and Testing', (Portcullis Press, UK, 1976).